A Data Fusion Technique for Wireless Ranging Performance Improvement

David Macii, *Member, IEEE*, Alessio Colombo, *Student Member, IEEE*, Paolo Pivato, *Student Member, IEEE*, and Daniele Fontanelli, *Member, IEEE*

***Abstract*—The increasing diffusion of mobile and portable devices provided with wireless connectivity makes the problem of distance measurement based on radio-frequency technologies increasingly important for the development of next-generation nomadic applications. In this paper, the performance limitations of two classic wireless ranging techniques based on received signal strength (RSS) and two-way time-of-flight (ToF) measurements, respectively, are analyzed and compared in detail. On the basis of this study, a data fusion algorithm is proposed to combine both techniques in order to improve ranging accuracy. The algorithm has been implemented and tested on the field using a dedicated embedded prototype made with commercial off-the-shelf components. Several experimental results prove that the combination of both techniques can significantly reduce measurement uncertainty. The results obtained with the developed prototype are not accurate enough for fine-grained position tracking in Ambient Assisted Living applications. However, the platform can be successfully used for reliable indoor zoning, e.g., for omnidirectional and adjustable hazard proximity detection. Most importantly, the proposed solution is absolutely general, and it is quite simple and light from the computational point of view. Accuracy could be further improved by using a more isotropic antenna and by integrating the ToF measurement technique at the lowest possible level on the same radio chip used for communication. Usually, this feature is not available in typical low-cost short-range wireless modules, e.g., for wireless sensor networks. Thus, the results of this research suggest that combining RSS with ToF measurements could be a viable solution for chip manufacturers interested in adding ranging capabilities to their radio modules.**

***Index Terms*—Distance measurement, estimation uncertainty, Kalman filtering, wireless sensor networks (WSNs).**

I. Introduction

In THE last years, wireless measurement techniques for indoor object positioning have become increasingly interesting in various applicative fields such as home automation, security, and Ambient Assisted Living (AAL). Unfortunately, most of the existing solutions suffer from limitations imposed by the line-of-sight (LOS) constraints, as they usually properly work only in a specified direction. As a consequence, they are very effective if the sensor-to-target bearing is known in advance or if complex pointing systems are used. Moreover, strongly directional sensors can be hardly used when power consumption is a concern. In fact, achieving both omnidirectionality and accuracy in the short range is notoriously quite hard, and consequently, it is still a hot research topic worldwide. Several approaches relying on different sensing technologies have been proposed for indoor positioning and ranging, e.g., based on laser rangefinders [1], ultrasound devices [2], infrared sensors [3], inertial platforms [4], and video cameras [5] or combinations thereof [6], [7]. Camera-based solutions are very effective in terms of accuracy, even in the presence of partial occlusions. However, they are not always usable because of privacy issues and because they suffer from scalability problems. To overcome the directional constraint of such systems, pan-tilt and omnidirectional cameras have been also proposed [8]. Their main drawback is the high computational burden when multiple targets have to be recognized and tracked. The most accurate approach is provided by laser scanning heads that also address the target pointing problem [9]. Unfortunately, these systems are very expensive. Radio frequency (RF)-based ranging techniques are inherently less sensitive to obstacles and dissipate less power than optical and ultrasound solutions. In addition, they could exploit the same wireless modules used for communication, and they are particularly suitable for wearable applications. In wireless RF ranging techniques, the distance between two objects is indirectly measured from some distance-related parameters of the RF signals. The two most common approaches are based on received signal strength (RSS) and message time-of-flight (ToF) measurements. The RSS-based methods rely on the relationship between the measured received signal power and the transmitter–receiver distance. If the transmitted power and the signal propagation model are known, the distance from the transmitter can be estimated by reversing the equation of the model. Usually, the RSS can be easily measured without additional circuitry, because most of the integrated wireless chips are natively equipped with an RSS indicator. RSS-based ranging has been widely analyzed in recent years, both theoretically and experimentally. An exhaustive empirical analysis of this method is available in [10] and [11]. The main drawback of RSS-based ranging is its considerable sensitivity to multipath and shadowing phenomena, which are particularly critical indoor for IEEE 802.15.4 wireless networks [12], [13]. Multipath propagation perturbs the ideal relationship between RSS values and distance, thus leading to nonmonotonic and space-varying measurement results [14]. Some researchers state that the performance of RSS-based methods cannot be significantly improved by means of signal processing techniques,

Manuscript received December 6, 2011; revised April 16, 2012; accepted June 14, 2012. Date of publication August 24, 2012; date of current version December 12, 2012. This work was supported by the Italian Ministry of University and Research through the PRIN 2008 project titled "Methodologies and measurement techniques for spatio-temporal localization in wireless sensor networks," (No. 2008TK5B55). The Associate Editor coordinating the review process for this paper was Dr. Jiong Tang.

The authors are with the DISI—Department of Information Engineering and Computer Science, University of Trento, 38123 Trento, Italy (e-mail: macii@disi.unitn.it).

Color versions of one or more of the figures in this paper are available online at http://ieeexplore.ieee.org.

Digital Object Identifier 10.1109/TIM.2012.2209918

since it is limited by the intrinsic variability of the RSS in the chosen environment [15]. However, other authors believe that the total uncertainty can be mitigated through subsequent refinements [16].

The ToF-based ranging methods rely on the measurement of the propagation time of a radio packet. In general, two alternative ToF-based ranging methods exist, i.e., the time-of-arrival (ToA) approach and the round-trip time (RTT) approach. The ToA method, also known as one-way ranging (OWR), is based on the estimation of the propagation time of a signal traveling between two wireless devices [17]. In particular, the estimated distance results from the product of the packet propagation time and the light speed. However, the OWR technique requires that the transmitter and the receiver are tightly synchronized (i.e., on the order of 1 ns or less for short-range communications), which is extremely challenging [18]. The RTT method instead, sometimes also referred to as two-way ranging (TWR), is based on the measurement of the time interval between the moment when a message is sent and the moment when the corresponding response message is received by the same device [19]. In this case, the ToF value is obtained by dividing the measured RTT by two after removing the time spent by the message on either node [20], [21]. Since the RTT is measured by the same device, no clock synchronization is required, and residual clock drifts can be removed through symmetric double-sided TWR [22]. Nowadays, the best available solutions based on RTT rely on ultrawideband signals [23], [24], as they proved to be less sensitive to multipath propagation issues. However, they require custom and sometimes power-hungry circuits that can be hardly used on wearable devices. Alternatively, solutions based on chirp spread spectrum (CSS) signals have been recently proposed, although their performance is not very clear [25], [26]. With other widely used wireless technologies (e.g., based on the standard IEEE 802.15.4), accuracy typically drops due to the large random jitter associated with time-interval measurements. However, in static conditions (namely at fixed distances), it can be improved through averaging or linear regression [27].

Whenever the presence of a moving object within a given area is enough to support decisions (e.g., as it may happen in some home automation applications), precise wireless ranging can just be replaced by proximity detection. Some common examples of proximity detectors are: photocells, magnetic, inductive or capacitive sensors, and RF identification (RFID) technologies [28], [29]. Despite the fact that proximity detection is simpler than ranging, achieving both low error rates and omnidirectionality is still quite challenging. In fact, infrared photocells have a limited field of view; inductive and capacitive sensors as well as passive RFID readers work only in the very short range, and active RFID solutions require a good relative orientation between antennas in order to assure adequate coupling. Furthermore, the proximity threshold, usually, can be hardly adjusted by the user according to the needs of the considered application. In this context, standard radio transceivers could also provide interesting alternatives for flexible proximity and zoning, provided that suitable techniques and algorithms are used [30].

In this paper, starting from an in-depth analysis of both RSS- and RTT-based ranging techniques (see Section II), a new data fusion algorithm combining the results of both techniques is presented in Section III. The proposed approach relies on the improvement of the algorithm reported in [30], and it has been implemented on a new custom embedded prototype, which is presented in Section IV. In Section V, after a detailed description of the experimental setup and a preliminary evaluation of the measurement uncertainty associated with either technique in static conditions, several experimental results in two orthogonal dynamic scenarios are reported. Finally, Section VI concludes the paper with some considerations about current limitations and perspectives of the proposed solution both for ranging and for flexible proximity detection.

II. Wireless Ranging Techniques

As stated in the Introduction, two different types of wireless RF ranging techniques are commonly used, i.e., those based on RSS and those relying on ToF values. With the RSS-based approach, the distance from the transmitting device can be estimated using the following expression [31]:

$$\boldsymbol{d}_R(t) = d_0 \cdot 10^{\frac{\boldsymbol{s}_0 - \boldsymbol{s}(t)}{10 \cdot \boldsymbol{\alpha}}} \tag{1}$$

where $\boldsymbol{s}(t)$ is a random variable describing the power (typically expressed in dBm) associated with a packet received by a given node at time t, $\boldsymbol{s}_0$ is the random variable modeling the RSS at a reference distance d_0, and $\boldsymbol{\alpha}$ is the *path loss* coefficient for the considered environment. While apparently simple, the distance measured through (1) is affected by multiple uncertainty contributions that may considerably alter measurement results. First of all, in indoor environments, $\boldsymbol{\alpha}$ typically deviates from the ideal value (i.e., 2 assuming the classic free-space attenuation model) as it ranges from ≈ 1.5 in a long corridor to ≈ 3 in furnished rooms [32]. Second, both $\boldsymbol{s}_0$ and $\boldsymbol{s}(t)$ are affected by multipath propagation and fading. In this respect, several research results confirm that the amplitude of a radio signal at various distances from a transmitter located in the same room exhibits a *Rice* rather than a *Rayleigh* distribution, because the LOS contribution is significantly larger than the signal replicas received after one or multiple reflections [33]. In particular, the so-called K-factor (namely, the ratio between the power of the LOS term and the total power of the other signal replicas) typically ranges from 2 to 5 [34]. In principle, this value should monotonically decrease, but in practice, it exhibits sudden oscillations [35], [36]. In addition, the antenna anisotropy and the limited resolution of the RSS detector integrated in most radio chips make uncertainty estimation even more difficult. If the law of propagation of uncertainty is applied to (1) under the assumption that all individual uncertainty terms are perfectly correlated and that the position-dependent systematic offsets are properly estimated and compensated [37], the worst case standard uncertainty is given by

$$u(\boldsymbol{d}_R(t)) = \frac{d_0 10^{\left(\frac{|\hat{s}_0 - \hat{s}(t)|}{10 \cdot \hat{\alpha}} - 1\right)}}{\hat{\alpha}} \cdot \left[u(\boldsymbol{s}_0) + u\left(\boldsymbol{s}(t)\right) + \frac{|\hat{s}_0 - \hat{s}(t)|}{\hat{\alpha}} u(\boldsymbol{\alpha}) \right] \tag{2}$$

where $u(\boldsymbol{s}(t))$, $u(\boldsymbol{s}_0)$, and $u(\boldsymbol{\alpha})$ are the standard uncertainties associated with the individual input quantities, whereas $\hat{s}_0$, $\hat{s}(t)$, and $\hat{\alpha}$ are the corresponding values measured at time t. Unfortunately, a trustworthy uncertainty stochastic model for the RSS is hard to find, and it is still an active research topic. Equation (2) suggests that the ranging uncertainty can be reduced by calibrating the system in different positions at the same reference distance d_0 from the target in order to make $u(\boldsymbol{s}_0)$ as little as possible. Observe that (2) tends to exponentially grow with the difference in RSS. This means that a properly calibrated RSS-based system could be potentially a good *proximity detector* with threshold d_0. However, it can be hardly used for accurate ranging at arbitrary distances.

The situation is quite different when the distance between two nodes is estimated through the ToF. In principle, the distance between the transmitter and the receiver can be easily estimated as follows:

$$\boldsymbol{d}_T(t) = \frac{c}{2}\left[\boldsymbol{\tau}(t) - \boldsymbol{o}_\tau(t)\right] \tag{3}$$

where $\boldsymbol{\tau}(t)$ is a random variable modeling the total RTT, c is the speed of light, and $\boldsymbol{o}_\tau(t)$ is the random temporal overhead given by the sum of

- the latency between the moment when a packet is timestamped on the sender side and the moment when the corresponding bit actually leaves the antenna;
- the time spent on the destination node to receive the incoming message and to reply with an acknowledgement (ACK) packet;
- the latency between the moment when the first bit of the ACK packet reaches the antenna and the moment when the message is timestamped by the receiver.

Note that (3) returns an accurate distance estimate only if

1) the node distance variation during the whole RTT is negligible;
2) $\boldsymbol{o}_\tau(t)$ is approximately constant so that it can be properly estimated and compensated.

While the first assumption is reasonably true for people moving indoor (i.e., quite slowly), the second one holds only if the various random latency contributions (particularly those due to the specific channel access mechanism employed) are negligible. Since, in general, this is not true, it is reasonable to assume that, due to the superimposition of multiple independent terms, the random fluctuations associated with $\boldsymbol{\tau}(t)$ and $\boldsymbol{o}_\tau(t)$ are quite large and normally distributed. In addition, the mean value of $\boldsymbol{o}_\tau(t)$ is expected to be much larger than the pure propagation time, but it can be estimated from the average of multiple RTT values collected when the destination node is placed at a known reference distance d_0. Accordingly, the worst case standard uncertainty associated with (3) after compensating possible position-dependent systematic offsets is simply given by [37]

$$u\left(\boldsymbol{d}_T(t)\right) = \frac{c}{2}\left[u\left(\boldsymbol{\tau}(t)\right) + u\left(\boldsymbol{o}_\tau(t)\right)\right] \tag{4}$$

where the standard uncertainty terms $u(\boldsymbol{\tau}(t))$ and $u(\boldsymbol{o}_\tau(t))$ are assumed to be stationary and perfectly correlated, and the wireless traffic is low enough as not to perturb the RTT significantly. In such conditions, (4) mainly depends on the message timestamping jitter both at the transmitting and at the receiving end. In particular, if the receiving timestamp is collected as soon as the first symbol or at least the first field of an incoming packet [e.g., the start frame delimiter (SFD)] is correctly detected, the RTT uncertainty is certainly quite smaller than the cumulative jitter associated with the reception of the whole message. In this case, the RTT measurement uncertainty depends on the random time at which the peak generated by the correlator at the input of the receiver crosses the detection threshold. Such a jitter is a function of the rising time of the correlation peak, and it depends on both the SNR at the receiver input and the chosen modulation scheme. However, if the LOS contribution is much stronger than the various multipath replicas and the distance between nodes is not so large as to make the SNR excessively low for reliable symbol detection, the jitter associated with the LOS correlation peak does not significantly change with distance. Usually, such a jitter is on the order of a few tens of nanoseconds if no special modulation schemes (e.g., CSS) are used [38]. Under such conditions, the relative impact of ToF uncertainty on ranging uncertainty tends to decrease as the distance between the transmitter and the receiver grows. However, it certainly grows back as soon as the SNR drops. In conclusion, from the previous analysis, it follows that the RSS-based ranging approach is preferable around the reference distance d_0, particularly in the very short range, where it is easier to have a better calibration. Conversely, the RTT-based technique looks more promising over a longer range. Several experimental results reported in Section V-A confirm this assumption. Therefore, combining both approaches is a sensible strategy to improve wireless ranging accuracy.

III. Data Fusion Algorithm for Distance Estimation

In order to perform object tracking, the distance between two nodes should be continuously measured over time. Assuming that one node is fixed, whereas the other is moving, the distance can be measured by either node (e.g., the moving device) as soon as it receives the response or acknowledgment message sent by its partner. Thus, every distance value estimated through either (1) or (3) is intrinsically event driven. If the communication between nodes periodically occurs, the time interval T_c between two consecutive messages received by the node measuring the distance can be regarded as the *sampling period* of the ranging system. In theory, T_c can be arbitrarily set by the user. The lower bound to T_c is given by the sum of the minimum RTT value including the time spent to process any sent or received packet and the computing time due to the distance estimation algorithm. Of course, T_c is generally subject to some fluctuations (e.g., due to timestamping jitter, channel access, or processing latency variations). However, if T_c is set much larger than these fluctuations, their effect on the performance of the digital ranging system is negligible, as shown in Section V-B.

As stated in Section II, in principle, the RSS and ToF data are affected by different uncertainty contributions. Therefore, the distance values estimated with (1) and (3) can be assumed to be just weakly correlated, and they can be merged in a variety of ways, e.g., by simply averaging both estimates or

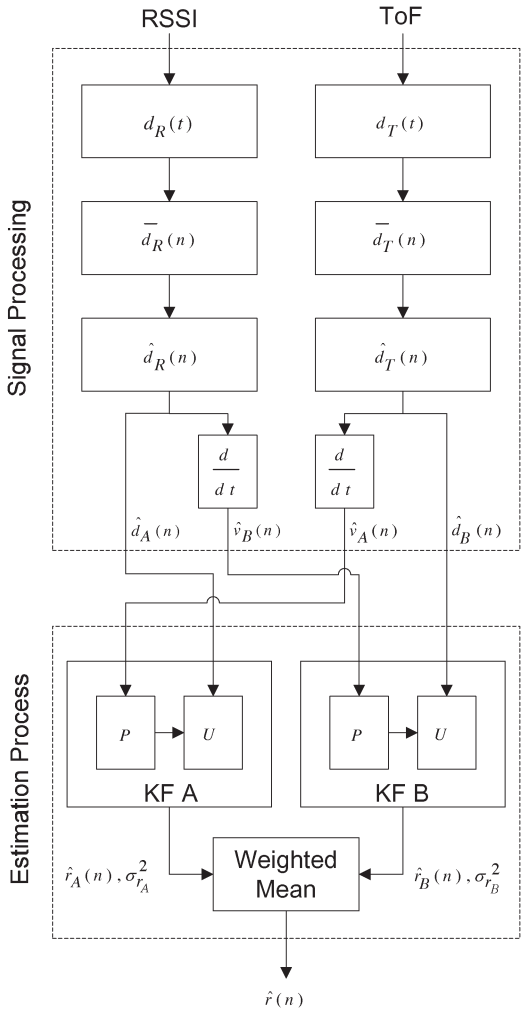

Fig. 1. Block diagram of the distance estimation algorithm based on RSS and ToF data fusion. The P and U initials in the diagram stand for *Prediction step* and *Update step*.

using one of them to measure the relative speed between nodes. In the following, the main steps of a new distance estimation algorithm based on RSS and ToF data fusion are reported. A visual description of this algorithm is offered in Fig. 1. The related symbols are defined in the following subsections.

A. Data Acquisition and Filtering

An essential preliminary step to improve ranging accuracy is data filtering. The purpose of this operation is not only to reduce the random fluctuations affecting raw measurement results (particularly the ToF values) but also to remove possible values that are not compatible with the movement of a real target (e.g., sudden large distance variations). Data filtering can be implemented in a variety of ways. However, the simultaneous presence of both wideband stationary noise and nonstationary disturbances suggests using an ad hoc solution based on the series of a linear filter with a nonlinear heuristic technique. As far as the linear part is concerned, a plain moving-average (MA) filter is used. In fact, not only is the MA filter extremely simple from the computational point of view, but it is also *optimal* in reducing the random wideband noise, since it has the smallest equivalent noise bandwidth among other finite-impulse response filters of the same order. In addition, it assures the sharpest step response [39], [40]. Moreover, unlike infinite-impulse response filters, the MA filter exhibits a perfect linear phase response, i.e., with no phase distortion and a constant and predictable group delay. The order M of the MA filters results from the tradeoff between four contrasting issues, i.e., output noise variance, filter bandwidth, available memory, and delay. The first two quantities decrease with M. However, if the filter bandwidth is too small, possible sharp direction changes of the moving target could be heavily filtered, thus degrading accuracy in dynamic conditions. In addition, the overall estimation delay should be lower than 1 or 2 s, in order not to excessively perturb the system responsiveness perceived by the user. Since the group delay of an MA filter in the analog domain is $(T_c \cdot M)/2$, by reducing T_c for a given value of M, filter responsiveness can be improved at no price in terms of accuracy. Thus, if M consecutive raw RSS and ToF data are filtered by an MA, the distance values resulting from either technique are given respectively by

$$\bar{d}_R(n) = d_0 \cdot 10^{\frac{\hat{s}_0 - \frac{1}{M}\sum_{i=0}^{M-1}\hat{s}(n-i)}{10\cdot\hat{\alpha}}} \tag{5}$$

$$\bar{d}_T(n) = \frac{c}{2}\left[\frac{1}{M}\sum_{i=0}^{M-1}\hat{\tau}(n-i) - \hat{o}_\tau\right] \tag{6}$$

where $\hat{s}_0$, $\hat{\alpha}$, and $\hat{o}_\tau$ are assumed to be previously estimated through calibration, while $\hat{s}(n)$ and $\hat{\tau}(n)$ are measured in real-time as soon as the nth ACK message is received. Of course, $\hat{s}(-1) = \cdots = \hat{s}(-M+1) = 0$ and $\hat{\tau}(-1) = \cdots = \hat{\tau}(-M+1) = 0$ by definition. Note that in (5) and (6), the MA is computed over raw measurement data *before* applying functions (1) and (3), as suggested in [37]. This approach is preferable in the case of indirect measurements based on nonlinear functional models, because it reduces the estimation bias caused by the intrinsic variance of the individual input quantities [41].

Unfortunately, as stated above, wideband noise is not the only uncertainty source in the considered measurement problem. Other position-dependent errors may significantly alter measurement results. In order to tackle this additional problem, a heuristic criterion based on human-motion constraints is used. In fact, the human speed in an indoor environment is usually smaller than $v_{\max} = 2$ m/s [42]. Therefore, any value returned by (5) and (6) can be considered as acceptable only if the variation from the last estimated distance does not exceed $\pm v_{\max} T_c$. In practice, this criterion leads to the definition of the following nonlinear filters:

$$\hat{d}_R(n) = \begin{cases} \hat{d}_R(n-1) + v_{\max} T_c & \bar{d}_R(n) - \hat{d}_R(n-1) \geq v_{\max} T_c \\ \hat{d}_R(n-1) - v_{\max} T_c & \bar{d}_R(n) - \hat{d}_R(n-1) \leq -v_{\max} T_c \\ \bar{d}_R(n) & \text{otherwise} \end{cases} \tag{7}$$

$$\hat{d}_T(n) = \begin{cases} \hat{d}_T(n-1) + v_{\max} T_c & \bar{d}_T(n) - \hat{d}_T(n-1) \geq v_{\max} T_c \\ \hat{d}_T(n-1) - v_{\max} T_c & \bar{d}_T(n) - \hat{d}_T(n-1) \leq -v_{\max} T_c \\ \bar{d}_T(n) & \text{otherwise.} \end{cases} \tag{8}$$

Note that the probability of saturation in (7) and (8) depends not only on the environmental and position-dependent disturbances but also on the order M of the MA filter. Some experimental data showing the effectiveness of the heuristic criterion are reported in Section V-A.

B. System Model

Let $r(t)$ be the LOS distance between two wireless nodes at time t. The dynamic of $r(t)$ can be described by the following simple linear kinematic model:

$$\begin{cases} \dot{r}(t) = v(t) \\ d(t) = r(t) \end{cases} \tag{9}$$

where the input $v(t)$ is the speed component of the moving object in the direction of the fixed node (in the following simply called as *relative radial speed*), and the distance $d(t)$ can be regarded as the output of the system. Given that either node can measure the values of $v(t)$ and $d(t)$ only when an ACK packet is received, system (9) can be discretized as follows:

$$\begin{cases} r(n+1) = r(n) + T_c v(n) + T_c \nu(n) \\ d(n) = r(n) + \epsilon(n) \end{cases} \tag{10}$$

where $r(n)$ and $v(n)$ are the distance and the radial speed values, respectively, after n message pairs are exchanged between nodes. It is worth emphasizing that the model defined by (10) holds both when T_c can be assumed to be constant and when T_c changes as a function of time. Of course, in the latter case, T_c should be also measured at run-time. The two discrete-time random sequences $\nu(\cdot)$ and $\epsilon(\cdot)$ in (10) model the effect of speed and distance measurement uncertainty. Both sequences depend on the superimposition of multiple nonstationary uncertainty contributions, e.g., the relative orientation of the antennas and the presence of obstacles or walls. As a consequence, $\nu(\cdot)$ and $\epsilon(\cdot)$ may exhibit time and/or space fluctuations that survive the preliminary filtering step. In particular, the position-dependent distance offsets randomly change when the target moves, thus becoming either positive or negative. Therefore, in a first approximation, $\nu(\cdot)$ and $\epsilon(\cdot)$ can be assumed to have zero-mean and time-varying variance in the spatio-temporal domain.

C. KF Definition

Since no clear assumptions can be made on the stochastic distribution of $\nu(\cdot)$ and $\epsilon(\cdot)$, finding an optimal dynamic state estimator of (10) is very difficult. For this reason, a simple but effective suboptimal approach was used to solve the estimation problem at hand. In fact, it is known that the Kalman filter (KF) is the best linear state estimator when either the process noise or the measurement uncertainty have unknown distributions [43]. A typical KF has a recursive structure that estimates the internal state of a linear dynamic system from a sequence of noisy measurement data. In particular, a KF consists of two main stages connected in a loop, i.e., the *prediction step* and the *update step*. If the superscript * is used to denote the *predicted* quantities, the *prediction* equations of the KF based on (10) are [43]

$$\begin{aligned} \hat{r}^*(n+1) &= \hat{r}(n) + T_c \hat{v}(n) \\ \hat{d}^*(n+1) &= \hat{r}^*(n+1) \\ \sigma_r^{*2}(n+1) &= \sigma_r^2(n) + T_c^2 \sigma_\nu^2(n) \end{aligned} \tag{11}$$

where $\sigma_r^2(n)$ and $\sigma_\nu^2(n)$ are the variance values associated with $\hat{r}(n)$ and $\nu(n)$, respectively, as soon as the nth ACK message is received. Since the system (10) is monodimensional, the covariance terms in (11) are just variances. While $\sigma_r^2(\cdot)$ is updated by the KF itself in the subsequent *update step*, $\sigma_\nu^2(\cdot)$ is estimated and modified in real-time using the collected input data (e.g., over a window of fixed size) due to the nonstationary behavior of $\nu(\cdot)$.

In the *update step*, it can be easily shown that [43]

$$\begin{aligned} \hat{r}(n+1) &= \hat{r}^*(n+1) + K(n+1)\left[\hat{d}(n+1) - \hat{d}^*(n+1)\right] \\ \sigma_r^2(n+1) &= \left[1 - \sigma_r^{*2}(n+1)\right] K(n+1) \end{aligned} \tag{12}$$

where $K(n+1) = \sigma_r^{*2}(n+1)[\sigma_r^{*2}(n+1) + \sigma_\epsilon^2(n+1)]^{-1}$ is the so-called *Kalman gain*, and $\sigma_\epsilon^2(n+1)$ is the variance of $\epsilon(n+1)$ when the $(n+1)$th ACK message is received. In practice, $\sigma_\epsilon^2(\cdot)$ can be estimated through a preliminary analysis of the distribution of $\epsilon(\cdot)$ in the considered environment, as described in Section V-A.

D. Data Fusion

According to (11) and (12), independent speed and position data are required to implement the KF. In particular, the relative radial speed between two nodes can be estimated as the ratio between the backward Euler difference of two consecutive distance measures and T_c. Given that RSS- and ToF-based distance values estimated with (7) and (8), respectively, can be assumed to be just weakly correlated, either (7) is used to measure $\hat{d}(\cdot)$ and (8) is employed to estimate $\hat{v}(\cdot)$ (*Kalman Filter A*, or KF A for brevity), or *vice versa* (*Kalman Filter B*, or KF B). In the former case, the relative radial speed to be used as input of (11) is given by $\hat{v}_A(n) = (\hat{d}_T(n) - \hat{d}_T(n-1))/T_c$, whereas the sequence of distance measures to be injected into (12) is simply $\hat{d}_A(n) = \hat{d}_R(n)$. Dually, in the latter case, radial speed and distance values result from $\hat{d}_B(n) = \hat{d}_T(n)$ and $\hat{v}_B(n) = (\hat{d}_R(n) - \hat{d}_R(n-1))/T_c$, respectively. In principle, only one of the two KFs should be used. However, both of them are suboptimal since the distribution of the uncertainty contributions is unknown and nonstationary both in time and in space. As a consequence, the most sensible approach is to run both KFs in parallel and then to weigh $\hat{r}_A(n)$ and $\hat{r}_B(n)$ using the reciprocal values of the respective variances. As a result, the measured distance is finally given by

$$\hat{r}(n) = \frac{\sigma_{r_B}^2(n)\hat{r}_A(n) + \sigma_{r_A}^2(n)\hat{r}_B(n)}{\sigma_{r_A}^2(n) + \sigma_{r_B}^2(n)}. \tag{13}$$

This way, the output mainly depends on the term with the smaller estimated uncertainty.

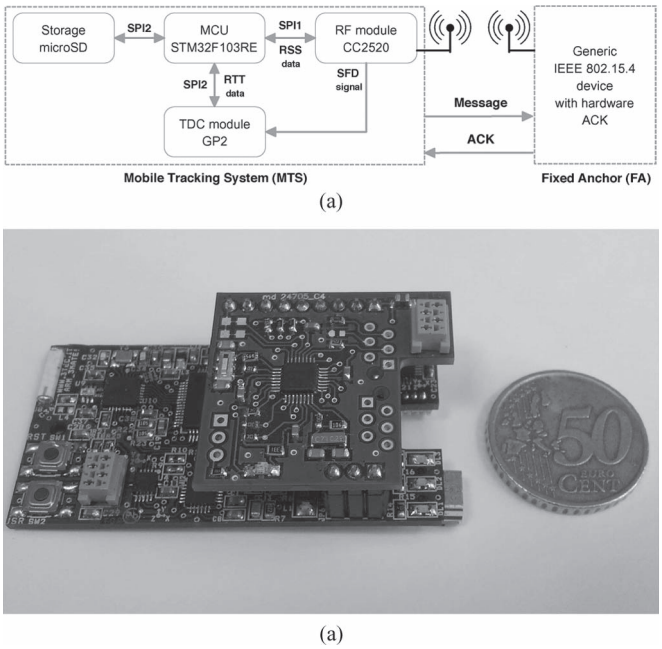

Fig. 2. (a) Functional block diagram and (b) snapshot of the MTS (by courtesy of Tretec S.r.l., Trento).

IV. Hardware Platform Description

In order to evaluate the performance of the data fusion algorithm described in Section III, a new wireless node prototype developed in cooperation with Tretec S.r.L., Trento, Italy, was used for all experimental activities. The block diagram and a snapshot of the node are shown in Fig. 2(a) and (b), respectively. The system results from the evolution of the node employed for similar experiments in [30], but it is smaller in size, and it is equipped with a faster microcontroller (MCU) and a larger memory. In particular, the node consists of

- a TI CC2520 RF transceiver compliant with the standard IEEE 802.15.4;
- a 32-bit STM32F103T8 MCU based on a 72-MHz ARM cortex M3 architecture with 20 kB of RAM and 64 kB of Flash memory;
- a tiny piggyback daughterboard provided with a time-to-digital converter (TDC) TDC-GP2 by Acam Mess Electronic with an RMS resolution of 50 ps;
- a 3.7-V 800-mAh rechargeable lithium-ion polymer battery;
- a chip antenna WE-MCA by Würth Elektronik located in one of the corners of the node prototype along with its own balun;
- a micro Secure Digital (SD) slot for data logging purposes;
- a USB port for node programming and battery charging.

The node, in the following simply referred to as *Mobile Tracking System* (MTS), is rectangular in shape with the following dimensions: $5.8 \times 3.0 \times 1.9$ cm. The last value refers to the thickness of the node including the battery. The MTS is able to measure both RSS and RTT data relative to a chosen *fixed anchor* (FA), which must be preliminary tuned on the same IEEE 802.15.4 channel used by the MTS. The lifetime of the node at room temperature when it is fully active (i.e., uninterruptedly used for high-rate distance measurements) is about 12 h when the transmission power is set to 0 dBm. The MCU is provided with two serial peripheral interfaces: one is used to handle and to exchange information with the transceiver, whereas the other one is linked to the TDC. The TDC is triggered by the rising edge of the SFD flag signal generated by the CC2520 when the first bit of the SFD field of an IEEE 802.15.4 message is sent. Similarly, the TDC is stopped by the rising edge of the same flag signal as soon as the SFD field of the corresponding ACK message is received. After the TDC is stopped, the corresponding RTT value is read by the MCU, followed by the RSS value associated with the ACK. Such data are buffered and timestamped by one of the timers of the MTS. If an excessive amount of time elapses between the edges starting and stopping the TDC, the TDC is reset, and the corresponding RTT value is discarded. In order to reduce the RTT latency as much as possible, the payload size of each message is set to the minimum specified in the standard IEEE 802.15.4 [44]. In addition, the MTS is configured to operate in a low-level mode, i.e., disabling the carrier sense multiple access with collision avoidance (CSMA-CA) mechanism. As a consequence, the transmission and the channel access times are not affected by the random back-off delays normally introduced by the media access control layer. In addition, the FA ACK response latency in a nonbeacon-enabled personal area network is deterministic and equal to the radio turnaround time [44]. It is worth highlighting that the FA is not required to be a special device, as instead it was in [30]. On the contrary, any IEEE 802.15.4-compliant node (e.g., a TelosB or a Tmote Sky) can play the role of the FA provided that its transceiver is configured to send ACK messages automatically, i.e., without MCU intervention. The T_c value can be arbitrarily set by the user, but, as stated in Section III, it must be larger than the sum of the worst case RTT, the total computational time of the MCU, and the time necessary to save the results into the micro SD memory card. Of course, faster transmission rates improve trajectory tracking and reduce estimation uncertainty for the same reasons described in [30]. By pressing a small button on the MTS, a user moving along a given trajectory can mark when he/she reaches specified points of interest, thus enabling a fair comparison between the estimated distance and the real one.

V. Experimental Results

Different types of experiments were conducted in the *Domotic Application Lab*, Department of Information Engineering and Computer Science, University of Trento. This laboratory consists of a 25-m^2 room furnished like a real living room (e.g., with a sofa, a table, some chairs, a TV set, and a small kitchen). All experiments were conducted by two trained researchers. The proposed testbed (which was purposely established and instrumented to support several projects dealing with domotics) offers the possibility to reproduce a real-world domestic indoor environment, while assuring repeatable conditions. At first, the MTS prototype was calibrated at known fixed distances. Afterward, the standard uncertainty associated

with raw distance measurement results as well as the average root-mean-square error (RMSE) in different positions of the room with and without using the heuristic filter were evaluated, as described in Section V-A. Finally, the accuracy of the MTS was analyzed in repeatable dynamic conditions, i.e., with the node carried by a user moving along given trajectories. The details of such experiments are described in Section V-B. All data were saved into the onboard SD memory and were eventually processed offline to extract interesting statistics about performance.

A. Uncertainty Evaluation of Individual Quantities

The standard uncertainty associated with individual RSS- and ToF-based measurements was evaluated with a Type-A approach [37], namely, with a statistical data analysis. A commercial Crossbow TelosB node configured as an FA was put on top of a 90-cm plastic pole at about 1 m from one of the walls of the room. The MTS prototype was put on another 90-cm pole that was placed in LOS conditions at various distances from the FA. Both nodes were tuned on the same IEEE 802.15.4 channel (i.e., channel 16 centered at 2.43 GHz) with a nominal transmission power equal to 0 dBm and with their antennas as parallel as possible in order to optimize the quality of the radio link. The MTS was calibrated in two steps. In the first one, about 5000 RSS and RTT raw values were collected at the reference distance $d_0 = 1$ m in four different orthogonal positions around the FA. The resulting average reference RSS value is $\hat{s}_0 = -55$ dBm with standard uncertainty $u(\hat{s}_0) = 4$ dBm. Similarly, the mean overhead latency estimated from (3) after averaging all RTT values collected at $d_0 = 1$ m is $\hat{o}_\tau = 433\,065$ ns with negligible standard uncertainty.

In the second step of the calibration procedure, about 5000 RSS and RTT values were collected by the MTS at 2, 3, 4, and 5 m from the FA. The path loss coefficient can be estimated through linear regression, after applying the base-10 logarithm function to both terms of (1). From this procedure, it follows that $\hat{\alpha} = 2.14$ with negligible uncertainty. In Fig. 3(a) and (b), the standard uncertainty and the RMSE patterns associated with $d_R(n)$ and $d_T(n)$, respectively, are plotted as a function of the real distance. The solid lines result from a Type-A uncertainty evaluation at different known distances from the FA, after removing the static position-dependent offsets. The dotted lines refer to the theoretical worst-case standard uncertainty values given by (2) and (4), respectively. Clearly, the theoretical and experimental uncertainty patterns are in good agreement. In particular, the uncertainty associated with the RSS data tends to grow with distance, whereas the uncertainty related to ToF-based estimates is approximately constant, as expected. The dashed lines in Fig. 3(a) and (b) represent the experimental RMSE patterns including the effect of both random fluctuations and position-dependent offsets. When the MTS is steadily located in the same place, the position-dependent offsets associated with each method are approximately systematic, and they cannot be removed by the preliminary filtering. Observe that the position-dependent offsets can significantly affect the RMSE, but their influence on RSS- and ToF-based measurement results can be different even when they refer to the same position. This justifies the use of an estimator based on the combination of dual techniques, such as the one proposed in this paper.

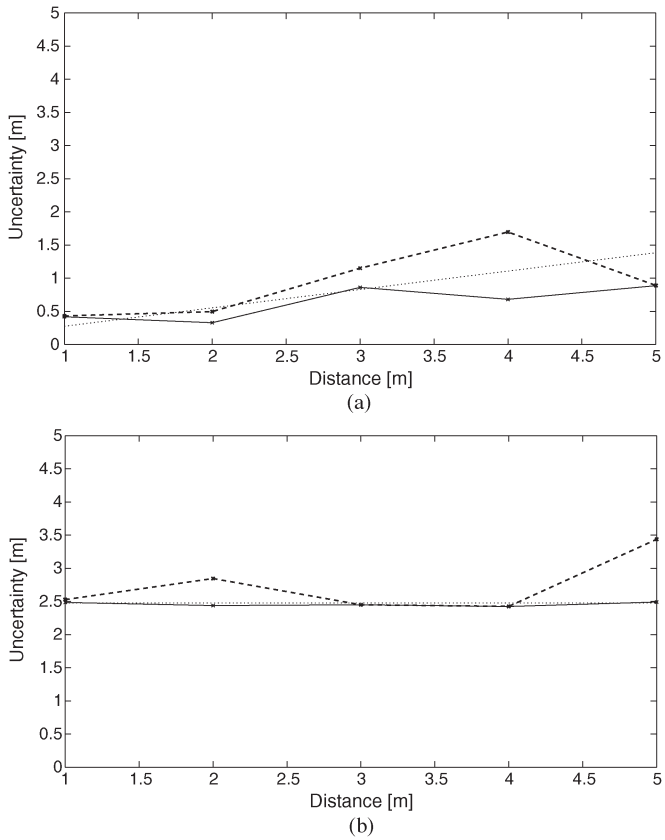

Fig. 3. Standard uncertainty and RMSE values associated with individual (a) RSS-based and (b) ToF-based distance measurements. The solid lines result from a Type-A uncertainty evaluation. The dotted lines in (a) and (b) refer to the worst case theoretical standard uncertainty values given by (2) and (4), respectively. Finally, the dashed lines represent the experimental RMSE values including the effect of both random fluctuations and position-dependent offsets.

Fig. 4 shows the probability that the saturation due to the heuristic criteria in (7) and (8) is actually activated when either the RSS values (dotted line) or the ToF values (solid line) are used for distance estimation. Both probability curves are computed as a function of the MA window size M over about 50 000 values collected at various known distances. The probability patterns show that the heuristic has a relevant impact when M is small, and it becomes less and less significant as M grows. This is quite obvious because with an MA computed over an increasingly large number of samples, all distance variations are heavily filtered. However, this also negatively affects the tracking capability of the MTS. Note that the heuristic is particularly useful in the case of ToF-based measurements. This is due to the fact that when M is small, the wideband noise affecting raw RTT values is so large as to trigger the heuristic with a very high probability.

Fig. 5 shows the average RMSE related to the same set of experiments as in Fig. 4. Different markers refer to RSS- and ToF-based distance estimators both with and without using the heuristic, i.e., based on (5)–(8), respectively. The benefits of

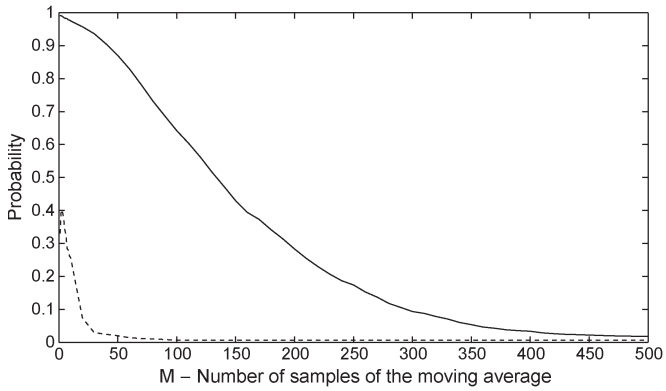

Fig. 4. Average probability of using the heuristic criterion as a function of the MA window size, when either the (dotted line) RSS values or the (solid line) ToF values are used for distance estimation.

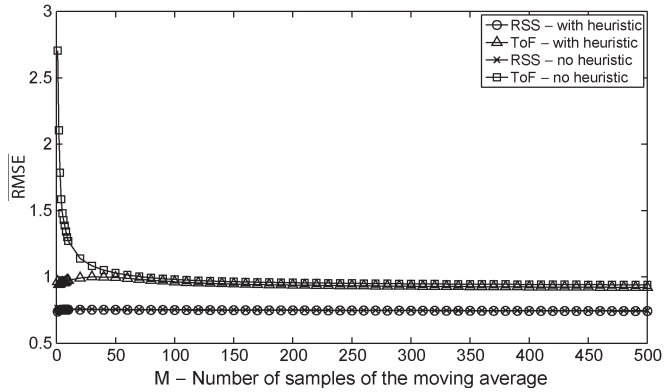

Fig. 5. Average RMSE patterns related to different RSS- and ToF-based distance estimators (i.e., MA filters only and MA filters enhanced with the heuristic).

the heuristic are evident for ToF-based distance measurements. In this case, the RMSE obtained with (8) is always smaller than the value resulting from (6). In addition, it converges to the asymptotic value with a smaller number of samples M. In this case, the residual error is clearly dominated by the average position-dependent offset. Observe that for $M \geq 100$, accuracy improvements are negligible. Therefore, it is pointless to compute an MA over a larger number of samples.

In the case of RSS-based distance measurements, the benefits of the heuristic criteria are typically minor. Nonetheless, in dynamic conditions, the heuristic can be very useful to remove sporadic large distance variations (i.e., outliers) due to abnormal RSS changes occurring in the considered environment.

B. Accuracy Analysis in Dynamic Conditions

The uncertainty analysis described in the previous subsection is essential for three main purposes:

1) To estimate the calibration parameters $\hat{s}_0$, $\hat{\alpha}$, and $\hat{o}_\tau$;
2) To define the size of the MA filter M;
3) To initialize both KFs.

As stated in Section V-A, the value of M should be set equal to 100. Since the MTS prototype is much faster than the platform described in [30], the minimum nominal value of T_c assuring both reliable radio communication and real-time data

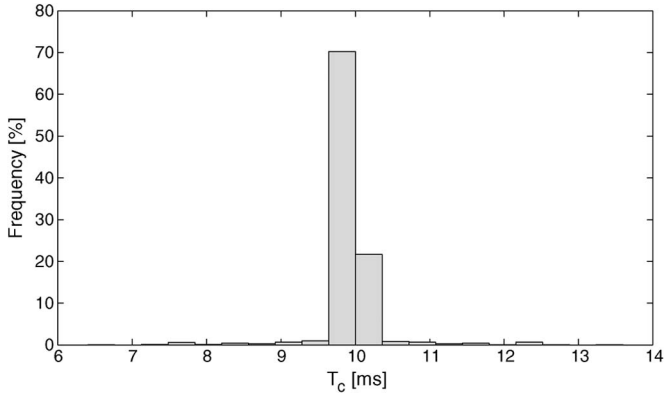

Fig. 6. Histogram of the measured sampling time values.

acquisition and processing is equal to 10 ms. Consequently, the group delay of the preliminary MA filter is just 0.5 s, i.e., low enough not to disturb the responsiveness perceived by the user. The random fluctuations affecting T_c are particularly small in the considered scenario. This is clearly visible in the histogram shown in Fig. 6, which reports the relative frequency of occurrence of the measured sampling periods out of several tens of thousands samples. Observe that more than 90% of values lie in the range 10 ± 0.2 ms. This is mainly due to the fact that the CSMA channel access mechanism is disabled and that the firmware is very optimized. A few outliers (below 1%) are caused by some lost packets.

The state variables of both KFs are initialized to 2.5 m with variance $\sigma^2_{r_A}(1) = \sigma^2_{r_B}(1) = 25$ m^2. The initial speed values instead are set equal to zero. While the speed variances $\sigma^2_{\nu_A}(\cdot)$ and $\sigma^2_{\nu_B}(\cdot)$ are estimated in real-time over the same M-long window used to compute the MA, the variances $\sigma^2_{\epsilon_A}(\cdot) = 4$ m^2 and $\sigma^2_{\epsilon_B}(\cdot) = 4$ m^2 associated with the measured distances are kept constant as they are mostly due to the position-dependent uncertainty contributions.

In order to test the performance of the algorithm in dynamic and realistic repeatable conditions, two kinds of orthogonal experiments were conducted in the *Domotic Application Lab*. In all cases, the FA was steadily kept on top of a fixed 90-cm plastic pole located in different positions, but always at about 1 m from the walls of the room. The MTS instead was manually held by the moving user just in front of the body at about 1 m from the floor, with the MTS and FA antennas reasonably parallel to each other and always in LOS conditions. No obstacles or bodies were used to steadily obstruct the LOS communication between the two wireless devices. However, the environment was perturbed by another person randomly moving in the room. In the first experimental session, a target person repeatedly moved forth and back along a 5-m straight-line radial trajectory until touching the FA. In order to make the trajectories as repeatable as possible, some reference adhesive labels were put on the floor at known distances from the FA. The values measured by the MTS in four check points (i.e., at 1.25, 2.5, 3.75, and 5 m in either direction) were marked by the user by pressing one of the buttons of the MTS, as soon as the user's leg treading on one of the labels was approximately vertical with a residual uncertainty of a few centimeters. The button press latency (including both the human reaction time

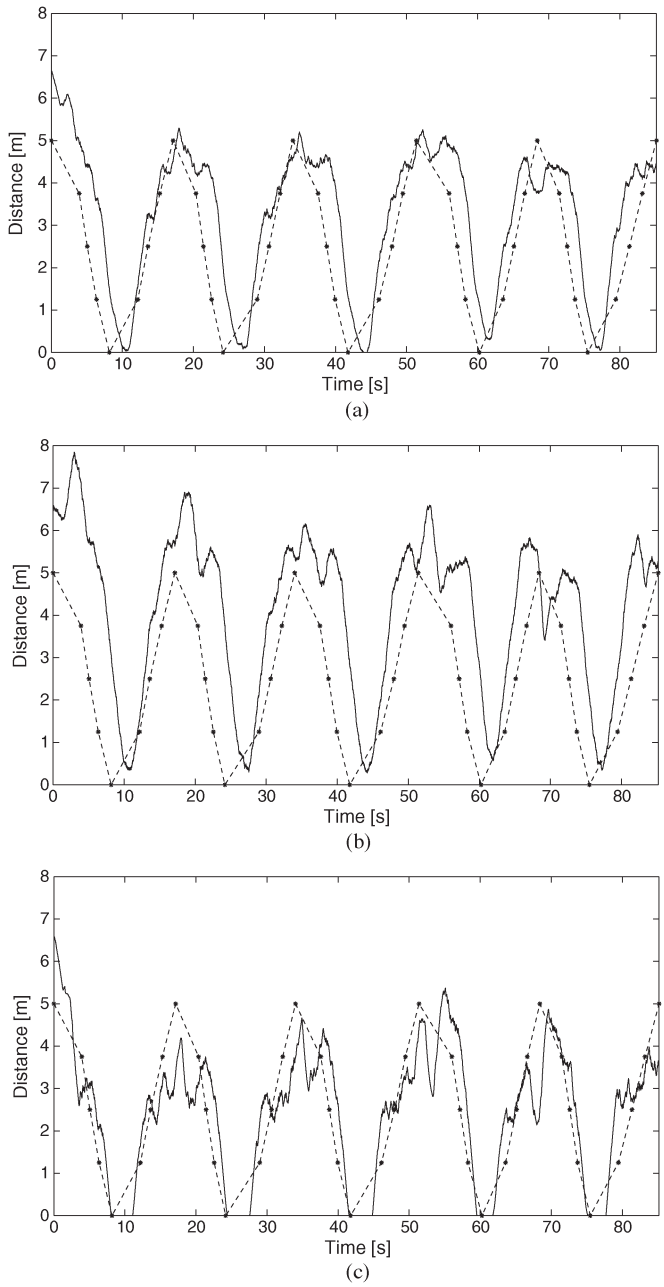

Fig. 7. Measurement results obtained with the (a) proposed algorithm, with the (b) KF A only, and with the (c) KF B only. In all cases, the target was moving forward and backward along a straight-line radial trajectory. The (dashed line) almost triangular waveform represents the real movement over time. The check points at 1.25, 2.50, 3.75, and 5 m from the FA are highlighted with star markers.

and the interrupt service processing time) is roughly 200 ms. At a speed of about 1 m/s, this means that the overall intrinsic uncertainty due to the chosen experimental setup is on the order of 20 cm. The results of one of these experiments in the time domain are shown in Fig. 7(a)–(c). In particular, Fig. 7(a) shows the distance estimated with the proposed algorithm, whereas the patterns in Fig. 7(b) and (c) refer to the output of KF A and KF B, respectively. The quasi-triangular waveforms (dashed lines) shown in each picture represent the real trajectory as a function of time. In addition, the star markers highlight the check points, namely, the moments when the button was pressed by the

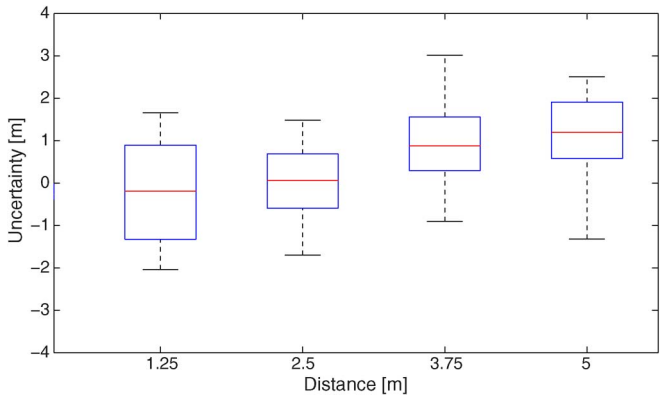

Fig. 8. Box-and-whiskers plot of the distance uncertainty at 1.25, 2.5, 3.75, and 5 m collected when the target moves along a 5-m straight-line forth-and-back trajectory.

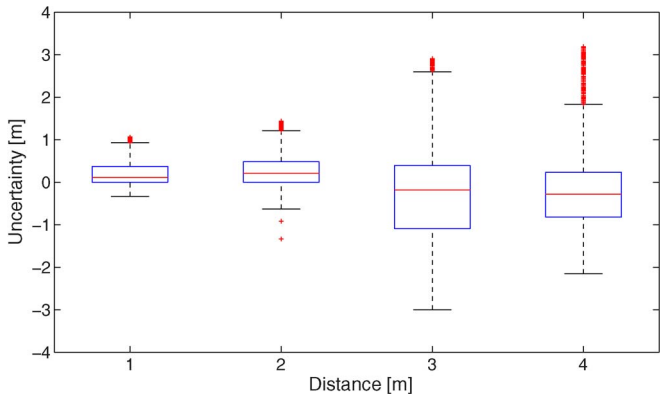

Fig. 9. Box-and-whiskers plot of the distance uncertainty at 1, 2, 3, and 4 m collected when the target repeatedly moves along a 2-m arc of a circle with the center in the FA.

moving user. Note that the proposed approach improves the estimation accuracy of either individual ranging technique.

The results of a more detailed analysis are reported in Fig. 8, which shows the box-and-whiskers plots of the errors associated with any of the four check points mentioned above. Each box refers to more than 50 data. Observe that the uncertainty is generally about 1 m. However, it may occasionally reach 2 m. Similar results are also confirmed by the second group of experiments, in which a target person repeatedly moved along a 2-m arc of a circle with the center in the FA and the radius equal to 1, 2, 3, and 4 m, respectively. Again, some stickers put on the floor and a wire of adjustable length used as a compass were used to keep the trajectories as stable and repeatable as possible. In this case, the intrinsic uncertainty due to the setup is on the order of a few centimeters. The corresponding box-and-whiskers plot is shown in Fig. 9. Observe that the worst case uncertainty tends to grow with distance, but it is quite low in the very short range. In applications where real users are involved, two main further intrinsic uncertainty contributions may seriously affect measurement results, i.e., possible changes in the relative orientation of MTS and FA antennas and poor LOS visibility (e.g., due to the posture of the person wearing the MTS or to other people steadily obstructing the LOS communication between MTS and FA). When such situations occur, uncertainty may grow from two to

three times as much. This is a common issue for all RF wireless ranging techniques, even those based on commercial platforms [45]. Nonetheless, the proposed data fusion algorithm is at least able to mitigate the detrimental effects of the uncertainty contributions described above, because the distance estimated through (13) prevailingly relies on the measurement result with the smaller overall variance. To further reduce this problem, the position of MTS and FAs should be always chosen so as to maximize nodes reciprocal visibility (e.g., with the MTS worn on a special hat and the FAs installed at least 2 m above the floor).

VI. Conclusion

This paper deals with a data fusion algorithm merging RSS and ToF measurement results in order to improve wireless ranging accuracy. Both approaches have been analyzed in detail in order to evaluate the main uncertainty contributions affecting either measurement procedure. The proposed algorithm has a general validity (i.e., independent of the chosen implementation), and it relies on two MA filters to reduce the input wideband noise, a heuristic criterion able to easily remove possible large position-dependent offsets, and two KFs that use RSS- and ToF-based measurement results in a complementary manner. Due to its moderate complexity, the algorithm could be integrated in future transceiver chips to support possible positioning services (e.g., for wireless sensor networks). At the moment, the algorithm has been implemented and tested on the field using a dedicated embedded system made up of commercial off-the-shelf (COTS) components. The estimated accuracy is generally about 1 m, but it can be so small as 50–60 cm around a given reference distance. Accordingly, such a distance can be also set as a threshold for adjustable and omnidirectional proximity detection. Unfortunately, the accuracy of the developed prototype is limited by the features of some hardware components, particularly the antenna that is not so isotropic as specified in the data sheet. Moreover, ToF measurement accuracy could be much better if message timestamping was done in the transceiver front end as soon as the first symbol of any packet is sent or received. However, this is not possible with COTS components. Due to the limitations above, the developed prototype cannot be used in AAL applications with tracking accuracy requirements on the order of a few tens of centimeters. Nevertheless, the system is accurate enough for reliable indoor zoning and proximity detection. For instance, the platform is going to be used in an AAL project where the staff assisting mentally disabled people (e.g., affected by Alzheimer's disease) should be alerted as soon as patients enter into potentially dangerous areas, e.g., within 1 m from windows, doors, staircases, or gas cookers.

Acknowledgment

The authors would like to thank Tretec S.r.L., Trento, for its constant support and F. Trenti for his essential contribution in collecting the preliminary data sets.

References

[1] D. Glas, T. Miyashita, H. Ishiguro, and N. Hagita, "Laser-based tracking of human position and orientation using parametric shape modeling," *Adv. Robot.*, vol. 23, no. 4, pp. 405–428, 2009.

[2] L. Angrisani, A. Baccigalupi, and R. Schiano Lo Moriello, "Ultrasonic time-of-flight estimation through unscented Kalman filter," *IEEE Trans. Instrum. Meas.*, vol. 55, no. 4, pp. 1077–1084, Aug. 2006.

[3] B. Andó and S. Graziani, "Multisensor strategies to assist blind people: A clear-path indicator," *IEEE Trans. Instrum. Meas.*, vol. 58, no. 8, pp. 2488–2494, Aug. 2009.

[4] B. Krach and P. Robertson, "Integration of foot-mounted inertial sensors into a Bayesian location estimation framework," in *Proc. 5th WPNC*, Hannover, Germany, Mar. 2008, pp. 55–61.

[5] E. Lobaton, R. Vasudevan, R. Bajcsy, and S. Sastry, "A distributed topological camera network representation for tracking applications," *IEEE Trans. Image Process.*, vol. 19, no. 10, pp. 2516–2529, Oct. 2010.

[6] F. Chavand, E. Colle, Y. Chekhar, and E. C. N'zi, "3-D measurements using a video camera and a range finder," *IEEE Trans. Instrum. Meas.*, vol. 46, no. 6, pp. 1229–1235, Dec. 1997.

[7] P. Vadakkepat and L. Jing, "Improved particle filter in sensor fusion for tracking randomly moving object," *IEEE Trans. Instrum. Meas.*, vol. 55, no. 5, pp. 1823–1832, Oct. 2006.

[8] A. Bonarini, P. Aliverti, and M. Lucioni, "An omnidirectional vision sensor for fast tracking for mobile robots," *IEEE Trans. Instrum. Meas.*, vol. 49, no. 3, pp. 509–512, Jun. 2000.

[9] A. Fod, A. Howard, and M. A. J. Mataric, "A laser-based people tracker," in *Proc. IEEE Int. Conf. Robot. Autom.*, May 2002, vol. 3, pp. 3024–3029.

[10] T. Pavani, G. Costa, M. Mazzotti, A. Conti, and D. Dardari, "Experimental results on indoor localization techniques through wireless sensors network," in *Proc. IEEE 63rd Veh. Technol. Conf.*, Melbourne, Austrialia, May 2006, vol. 2, pp. 663–667.

[11] K. Benkic, M. Malajner, P. Planinsic, and Z. Cucej, "Using RSSI value for distance estimation in wireless sensor networks based on ZigBee," in *Proc. IEEE Int. Conf. Syst., Signals Image Process.*, Jun. 2008, pp. 303–306.

[12] D. Lymberopoulos, Q. Lindsey, and A. Savvides, "An empirical characterization of radio signal strength variability in 3-D IEEE 802.15.4 networks using monopole antennas," in *Wireless Sensor Networks*. Berlin, Germany: Springer, 2006, pp. 326–341.

[13] K. Whitehouse, C. Karlof, and D. Culler, "A practical evaluation of radio signal strength for ranging-based localization," *SIGMOBILE Mob. Comput. Commun. Rev.*, vol. 11, no. 1, pp. 41–52, Jan. 2007.

[14] P. Pivato, L. Palopoli, and D. Petri, "Accuracy of RSS-based centroid localization algorithms in an indoor environment," *IEEE Trans. Instrum. Meas.*, vol. 60, no. 10, pp. 3451–3460, Oct. 2011.

[15] E. Elnahrawy, L. Xiaoyan, and R. P. Martin, "The limits of localization using signal strength: A comparative study," in *Proc. IEEE SECON*, Santa Clara, CA, Oct. 2004, pp. 406–414.

[16] A. Savvides, H. Park, and M. B. Srivastava, "The bits and flops of the n-hop multilateration primitive for node localization problems," in *Proc. ACM Int. Workshop Wireless Sens. Netw. Appl.*, Atlanta, GA, 2002, pp. 112–121.

[17] I. Guvenc and C.-C. Chong, "A survey on TOA based wireless localization and NLOS mitigation techniques," *IEEE Commun. Surveys Tuts.*, vol. 11, no. 3, pp. 107–124, Third Quarter, 2009.

[18] J. X. Lee, Z. W. Lin, P. S. Chin, and K. P. Yar, "One-way ranging time drift compensation for both synchronized and non-synchronized clocks," in *Proc. Int. Conf. Syst. Sci. Eng.*, Taipei, Taiwan, Jul. 2010, pp. 327–331.

[19] Y. Jiang and V. Leung, "An asymmetric double sided two-way ranging for crystal offset," in *Proc. Int. Symp. Signals, Syst. Electron.*, Montreal, QC, Canada, Aug. 2007, pp. 525–528.

[20] D. Wang, R. Kannan, L. Wei, and B. Tay, "Time of flight based two way ranging for real-time locating systems," in *Proc. IEEE Conf. Robot. Autom. Mechatron.*, Singapore, Jun. 2010, pp. 199–205.

[21] M. Kwak and J. Chong, "A new double two-way ranging algorithm for ranging system," in *Proc. 2nd IEEE Int. Conf. Netw. Infrastructure Digital Content*, Beijing, China, Sep. 2010, pp. 470–473.

[22] IEEE Standard for Information Technology—Telecommunications and Information Exchange Between Systems—Local and Metropolitan Area Networks—Specific Requirement Part 15.4: Wireless Medium Access Control (MAC) and Physical Layer (PHY) Specifications for Low-Rate Wireless Personal Area Networks (WPANs), IEEE Std., 2007.

[23] A. De Angelis, M. Dionigi, A. Moschitta, and P. Carbone, "A low-cost ultra-wideband indoor ranging system," *IEEE Trans. Instrum. Meas.*, vol. 58, no. 12, pp. 3935–3942, Dec. 2009.

[24] J. Zhang, P. V. Orlik, Z. Sahinoglu, A. F. Molisch, and P. Kinney, "UWB systems for wireless sensor networks," *Proc. IEEE*, vol. 97, no. 2, pp. 313–331, Feb. 2009.
[25] C. Röhrig and M. Müller, "Localization of sensor nodes in a wireless sensor network using the nanoLOC TRX transceiver," in *Proc. IEEE 69th Veh. Technol. Conf.*, Barcelona, Spain, Apr. 2009, pp. 1–5.
[26] E. Karapistoli, F.-N. Pavlidou, I. Gragopoulos, and I. Tsetsinas, "An overview of the IEEE 802.15.4a standard," *IEEE Commun. Mag.*, vol. 48, no. 1, pp. 47–53, Jan. 2010.
[27] G. Santinelli, R. Giglietti, and A. Moschitta, "Self-calibrating indoor positioning system based on ZigBee devices," in *Proc. IEEE Int. Instrum. Meas. Technol. Conf.*, Singapore, May 2009, pp. 1205–1210.
[28] D. Sanders, S. Mukhi, M. Laskowski, M. Khan, B. Podaima, and R. McLeod, "A network-enabled platform for reducing hospital emergency department waiting times using an RFID proximity location system," in *Proc. IEEE ICSENG*, NV, Aug. 2008, pp. 538–543.
[29] J. Song, C. T. Haas, and C. H. Caldas, "A proximity-based method for locating RFID tagged objects," *Adv. Eng. Inf.*, vol. 21, no. 4, pp. 367–376, Oct. 2007.
[30] D. Macii, P. Pivato, and F. Trenti, "A robust wireless proximity detection techniques based on RSS and ToF measurements," in *Proc. IEEE Int. Workshop Meas. Netw.*, Anacapri, Italy, Oct. 2011, pp. 31–36.
[31] T. S. Rappaport, *Wireless Communications—Principles and Practice*, 2nd ed. Upper Saddle River, NJ: Prentice-Hall PTR, Dec. 2001.
[32] J. D. Gibson, *The Mobile Communication Handbook*, 1st ed. New York: CRC Press, Feb. 1996.
[33] Y. Lustmann and D. Porrat, "Indoor channel spectral statistics, K-factor and reverberation distance," *IEEE Trans. Antennas Propag.*, vol. 58, no. 11, pp. 3685–3692, Nov. 2010.
[34] V. Nikolopoulos, M. Fiacco, S. Stavrou, and S. R. Saunders, "Narrowband fading analysis of indoor distributed antenna systems," *IEEE Antennas Wireless Propag. Lett.*, vol. 2, no. 1, pp. 89–92, Jan. 2003.
[35] D. Puccinelli and M. Haenggi, "Multipath fading in wireless sensor networks: Measurements and interpretation," in *Proc. Int. Conf. Wireless Commun. Mobile Comput.*, Vancouver, BC, Canada, Jul. 2006, pp. 1039–1044.
[36] S. Wyne, T. Santos, F. Tufvesson, and A. F. Molisch, "Channel measurements of an indoor office scenario for wireless sensor applications," in *Proc. IEEE Global Telecommun. Conf.*, Washington, DC, Nov. 2007, pp. 3831–3836.
[37] "Evaluation of Measurement Data—Guide to the Expression of Uncertainty in Measurement," JCGM, Geneva, Switzerland, JCGM 100:2008, Sep. 2008.
[38] C. De Dominicis, P. Ferrari, A. Flammini, and E. Sisinni, "Wireless sensors exploiting IEEE802.15.4a for precise timestamping," in *Proc. IEEE Int. Symp. Precision Clock Synchronization Meas. Control Commun.*, Portsmouth, NH, Sep./Oct. 2010, pp. 48–54.
[39] S. W. Smith, *Digital Signal Processing: A Practical Guide for Engineers and ScientistsBuslingfon, MA*. Oxford, U.K.: Newnes, Nov. 2002.
[40] F. Stefani, M. Moschitta, D. Macii, P. Carbone, and D. Petri, "Fast estimation of ADC nonlinearities using the Sinewave Histogram Test," *Measurement*, vol. 39, no. 3, pp. 232–237, Apr. 2006.
[41] D. Macii, L. Mari, and D. Petri, "Comparison of measured quantity value estimators in nonlinear models," *IEEE Trans. Instrum. Meas.*, vol. 59, no. 1, pp. 238–246, Jan. 2010.
[42] G. Arechavaleta, J.-P. Laumond, H. Hicheur, and A. Berthoz, "The nonholonomic nature of human locomotion: A modeling study," in *Proc. 1st IEEE/RAS-EMBS Int. Conf. Biomed. Robot. Biomechatron.*, Pisa, Italy, Feb. 2006, pp. 158–163.
[43] Y. Bar-Shalom, X. Rong Li, and T. Kirubarajan, *Estimation With Applications to Tracking and Navigation: Theory, Algorithms and Software*. Hoboken, NJ: Wiley, 2002.
[44] *IEEE Wireless Medium Access Control (MAC) and Physical Layer (PHY) Specifications for Low-Rate Wireless Personal Area Networks (WPANs)*, IEEE Std. 802.15.4, 2006.
[45] P. Pivato, S. Dalpez, and D. Macii, "Performance evaluation of chirp spread spectrum ranging for indoor embedded navigation systems," in *Proc. IEEE SIES*, Karlsruhe, Germany, Jun. 2012, pp. 1–4.

David Macii (S'01–M'06) received the five-year degree in electronic engineering and the Ph.D. degree in information engineering from the University of Perugia, Perugia, Italy, in 2000 and 2003, respectively.

He did research with the Department of Digital Networks, German Aerospace Centre DLR, Munich, Germany, in 2000; with the Applied DSP and VLSI Research Group, University of Westminster, London, U.K., in 2002; with the Advanced Learning and Research Institute, University of Lugano, Lugano, Switzerland, between 2003 and 2005; and with the Berkeley Wireless Research Center, University of California, Berkeley, between 2009 and 2010 as a Fulbright Research Scholar. Since January 2005, he has been an Assistant Professor in Electronics and Measurement Science with the Department of Information Engineering and Computer Science (DISI), University of Trento, Trento, Italy. His research interests include the design, implementation, and characterization of embedded systems, with a special emphasis on power reduction and estimation techniques, wireless sensor networks, and data acquisition systems.

Alessio Colombo (S'07) received the B.S. and M.S. degrees in computer science from the University of Trento, Trento, Italy, in 2007 and 2010, respectively. He is currently working toward the Ph.D. degree in information technologies and computer science in the Department of Information Engineering and Computer Science, University of Trento.

In 2012, he was a Visiting Researcher with the National Institute for Research in Computer Science and Control (INRIA), Rennes, France. His research interests include embedded system control and design, indoor localization, and motion planning algorithms for autonomous robots.

Paolo Pivato (S'05) received the B.S. and M.S. degrees in telecommunications engineering from the University of Trento, Trento, Italy, in 2004 and 2009, respectively. He is currently working toward the Ph.D. degree in information and communication technologies in the Department of Information Engineering and Computer Science, University of Trento.

His main research interests include localization in wireless sensor networks as well as embedded systems design and development.

Daniele Fotanelli (M'09) received the M.S. degree in information engineering and the Ph.D. degree in automation, robotics and bioengineering from the University of Pisa, Pisa, Italy, in 2001 and 2006, respectively.

From 2006 to 2007, he was a Visiting Scientist with the Vision Lab, University of California at Los Angeles, Los Angeles. From 2007 to 2008, he was an Associate Researcher with the Interdepartmental Research Center "E. Piaggio," University of Pisa. Since 2008, he has been an Associate Researcher with the Department of Information Engineering and Computer Science, University of Trento, Trento, Italy. His research interests include robotics and visual servoing, embedded system control, wireless sensor networks, and networked and distributed control.